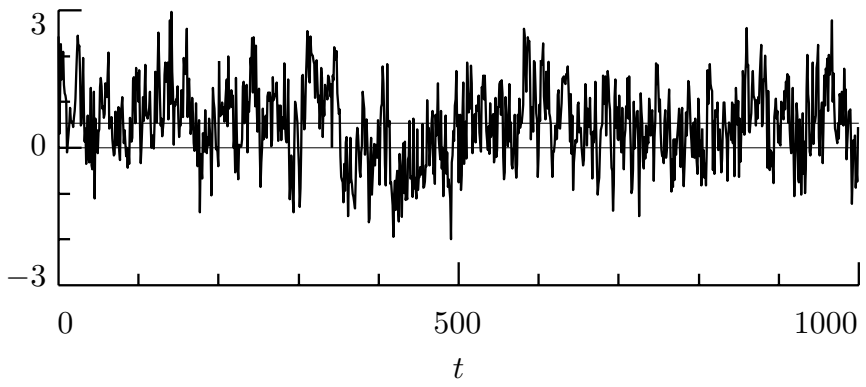

Figure 300. Realization of a fractional Gaussian noise (FGN) process with self-similarity parameter $H = 0.9$. The sample mean of approximately 0.53 and the true mean of zero are indicated by the thin horizontal lines.

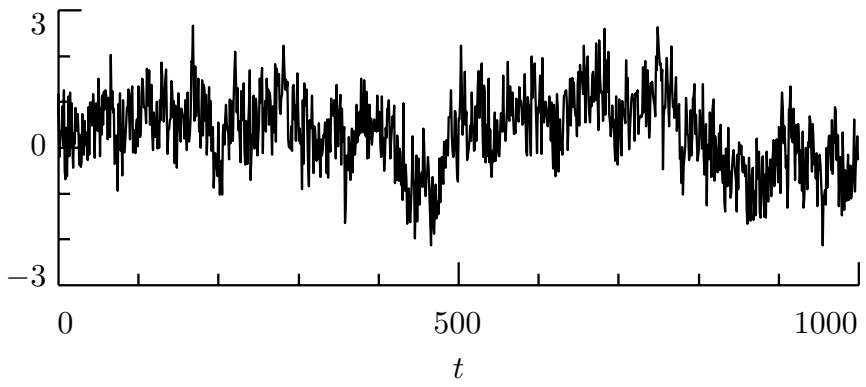

Figure 301. Realization of a stochastic process whose first order backward difference is an FGN process with self-similarity parameter $H = 0.1$. Depending upon its precise definition, the variance for this process is either infinite for all t or is time dependent and increases to infinity as $|t|$ goes to infinity.

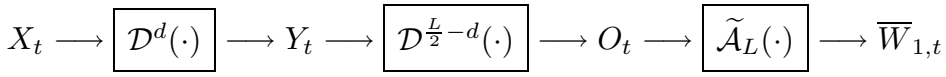

Figure 305. Flow diagram depicting filtering of $\{X_t\}$ using the Daubechies MODWT wavelet filter $\{\tilde{h}_l\}$ to obtain $\overline{W}_{1,t}$. The actual filter can be decomposed into a cascade involving three filters (indicated above by their squared gain functions $\mathcal{D}^d(\cdot)$, $\mathcal{D}^{\frac{L}{2}-d}(\cdot)$ and $\widetilde{\mathcal{A}}_L(\cdot)$). By assumption the dth order backward difference of $\{X_t\}$ is a stationary process $\{Y_t\}$, while the wavelet filter has a width $L \geq 2d$ and hence implicitly involves $L/2$ backward difference filters $\mathcal{D}(\cdot)$. When $L = 2d$, the processes $\{Y_t\}$ and $\{O_t\}$ are identical (the filter $\mathcal{D}^0(\cdot)$ is taken to be a 'do nothing' filter); when $L > 2d$, we obtain $\{O_t\}$ by taking $\frac{L}{2} - d$ successive backward differences of $\{Y_t\}$. In either case, the process $\{O_t\}$ is then subjected to the smoothing filter $\widetilde{\mathcal{A}}_L(\cdot)$, yielding the first level wavelet coefficient process $\{\overline{W}_{1,t}\}$.

δ	$L = 2$	$L = 4$	$L = 6$	$L = 8$
$-1/2$	0.85	0.89	0.91	0.92
$-1/4$	0.81	0.86	0.89	0.90
$-1/8$	0.78	0.84	0.87	0.89
0	0.75	0.82	0.85	0.87
$1/8$	0.72	0.80	0.83	0.86
$1/4$	0.68	0.77	0.81	0.84
$1/2$	0.61	0.72	0.77	0.80
1	0.50	0.61	0.67	0.71
$3/2$	—	0.52	0.58	0.62

Table 310. Asymptotic relative efficiencies (AREs) of the DWT-based estimator $\hat{\hat{\nu}}^2_X(\tau_1)$ with respect to the MODWT-based estimator $\hat{\nu}^2_X(\tau_1)$ for various combinations of FD processes and Daubechies wavelet filters. Note that an ARE of less than unity implies that $\hat{\nu}^2_X(\tau_1)$ has smaller large sample variance than $\hat{\hat{\nu}}^2_X(\tau_1)$.

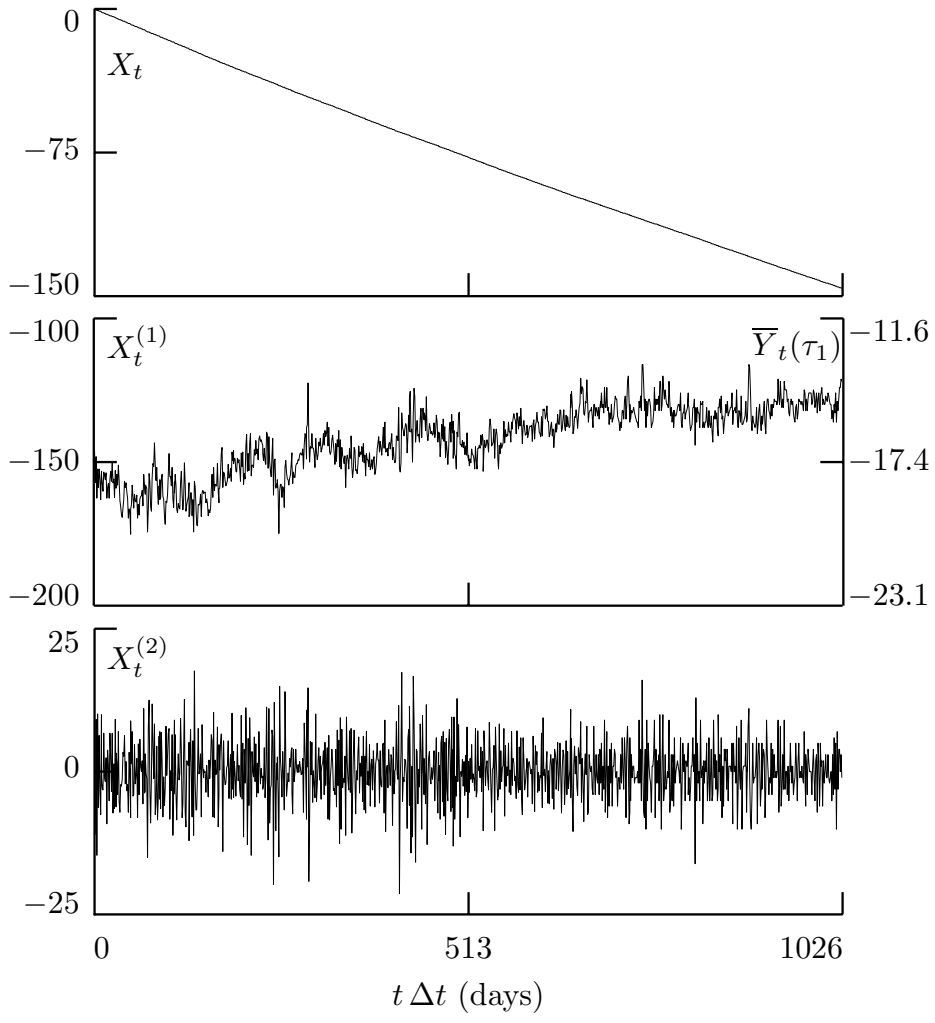

Figure 318. Plot of differences in time $\{X_t\}$ as kept by clock 571 (a cesium beam atomic clock) and as kept by the time scale UTC(USNO) maintained by the US Naval Observatory, Washington, DC (top plot); its first backward difference $\{X_t^{(1)}\}$ (middle); and its second backward difference $\{X_t^{(2)}\}$ (bottom). In the middle plot, $\overline{Y}_t(\tau_1)$ denotes the τ_1 average fractional frequency deviates (given in parts in 10^{13}) – these are defined by Equation (321c) and are proportional to $X_t^{(1)}$.

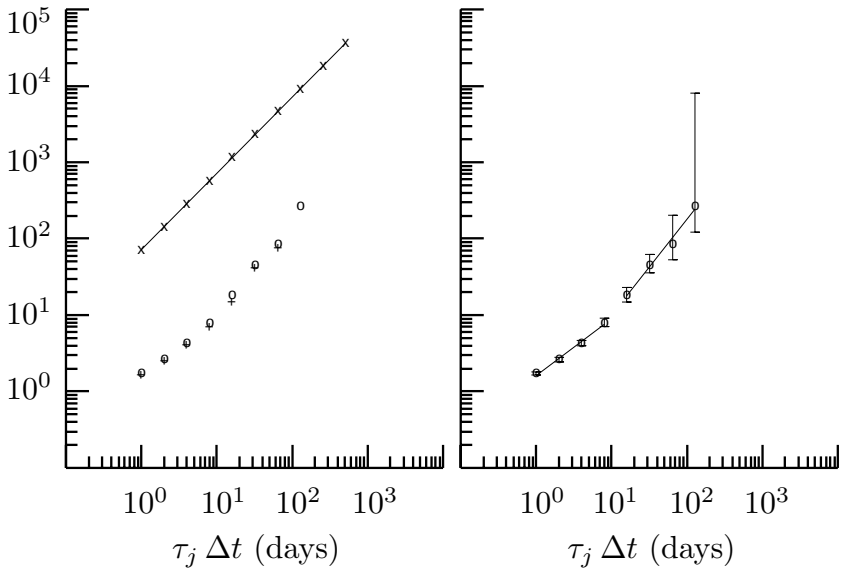

Figure 319. Square roots of wavelet variance estimates for atomic clock time differences $\{X_t\}$ based upon the unbiased MODWT estimator and the following wavelet filters: Haar (x's in left-hand plot, through which a least squares line has been fit), D(4) (circles in left- and right-hand plots) and D(6) (pluses in left-hand plot). The 95% confidence intervals in the second plot are the square roots of intervals computed using Equation (313c), with η given by $\hat{\eta}_1$ of Equation (313d) for $j = 1, \ldots, 6$ and by η_3 of Equation (314c) for $j = 7, 8$. The actual values for the various $\hat{\nu}_X(\tau_j)$ are listed on the Web site for this book – see page *xiv*.

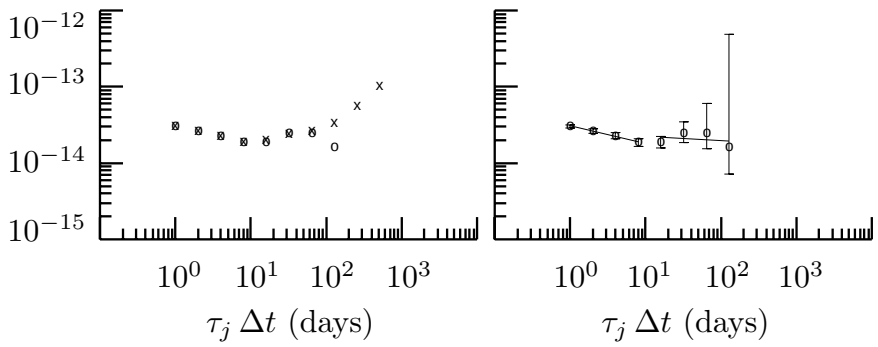

Figure 322. Square roots of wavelet variance estimates for atomic clock one day average fractional frequency deviates $\{\overline{Y}_t(\tau_1)\}$ based upon the unbiased MODWT estimator and the following wavelet filters: Haar (x's in left-hand plot) and D(4) (circles in left and right-hand plots). The actual values for $\hat{\nu}_{\overline{Y}}(\tau_j)$ are listed on the Web site for this book – see page *xiv*.

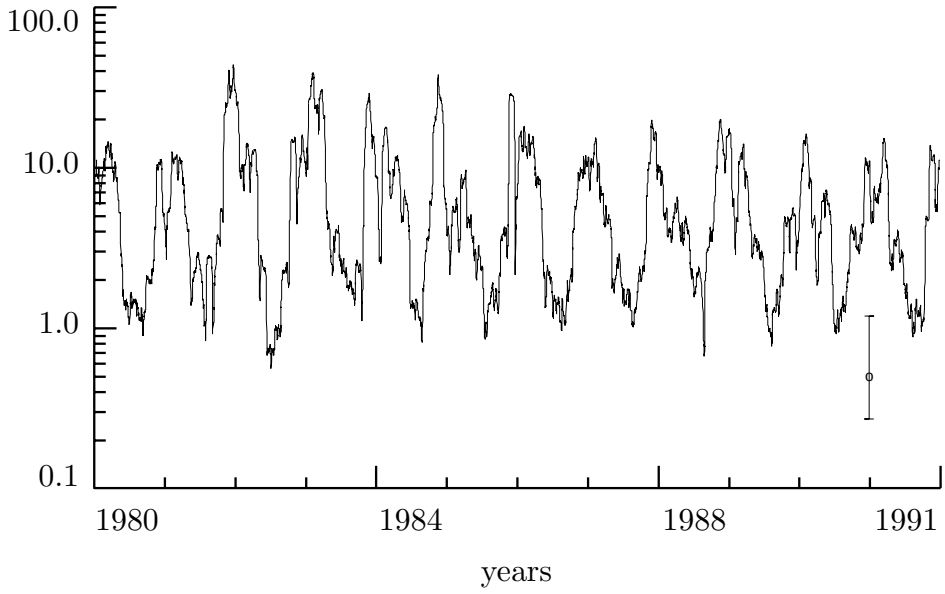

Figure 324. Estimated time-dependent LA(8) wavelet variances for physical scale $\tau_2 \, \Delta t = 1$ day for the Crescent City subtidal sea level variations of Figure 186, along with a representative 95% confidence interval based upon a hypothetical wavelet variance estimate of 1/2 and a chi-square distribution with $\nu = 15.25$ (see text for details).

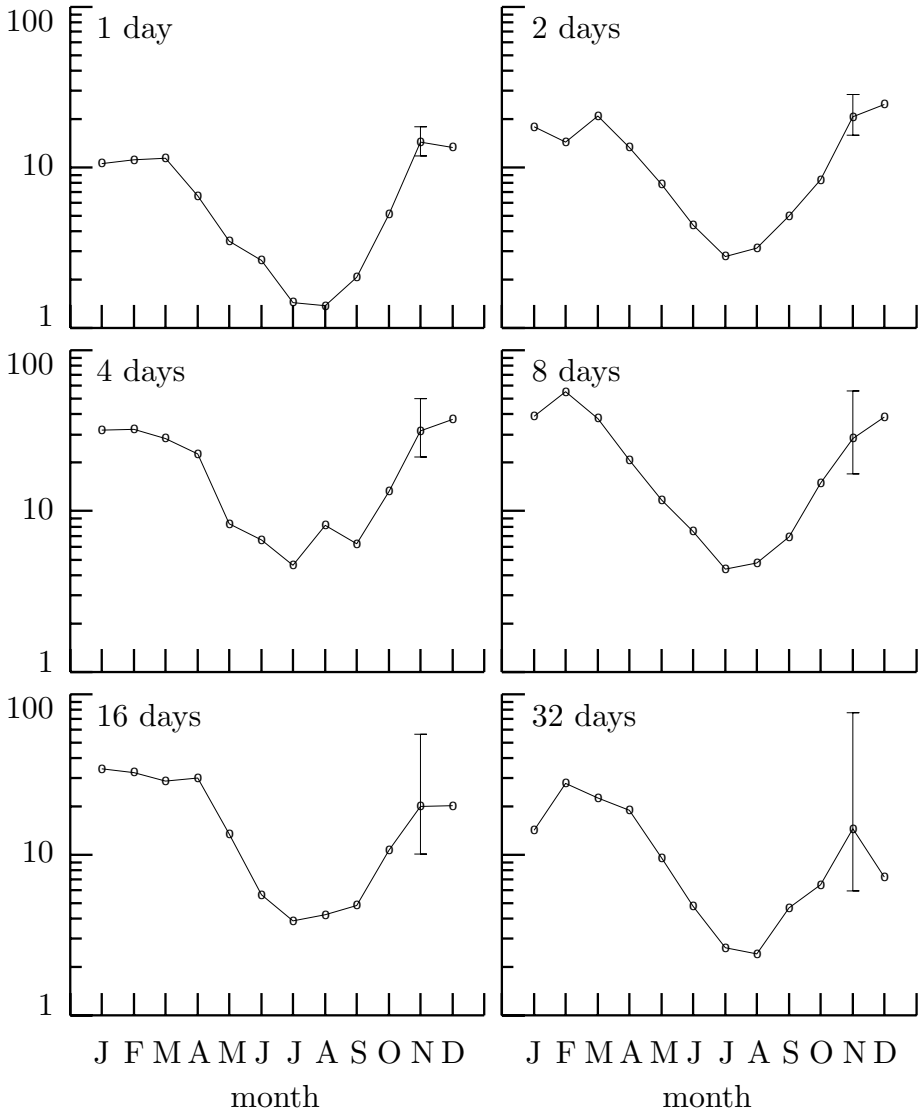

Figure 326. Estimated LA(8) wavelet variances for physical scales $\tau_j \, \Delta t = 2^{j-2}$ days, $j = 2, \ldots, 7$, grouped by calendar month for the subtidal sea level variations of Figure 186.

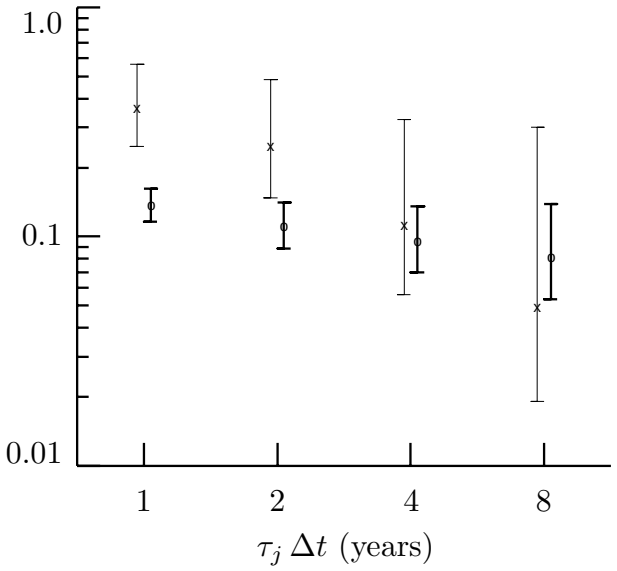

Figure 327. Estimated Haar wavelet variances for the Nile River minima time series before and after year 715.5 (x's and o's, respectively), along with 95% confidence intervals (thin and thick lines, respectively) based upon a chi-square approximation with EDOFs determined by η_3 of Equation (314c). The actual values for $\hat{\nu}_X^2(\tau_j)$ are listed on the Web site for this book – see page *xiv*.

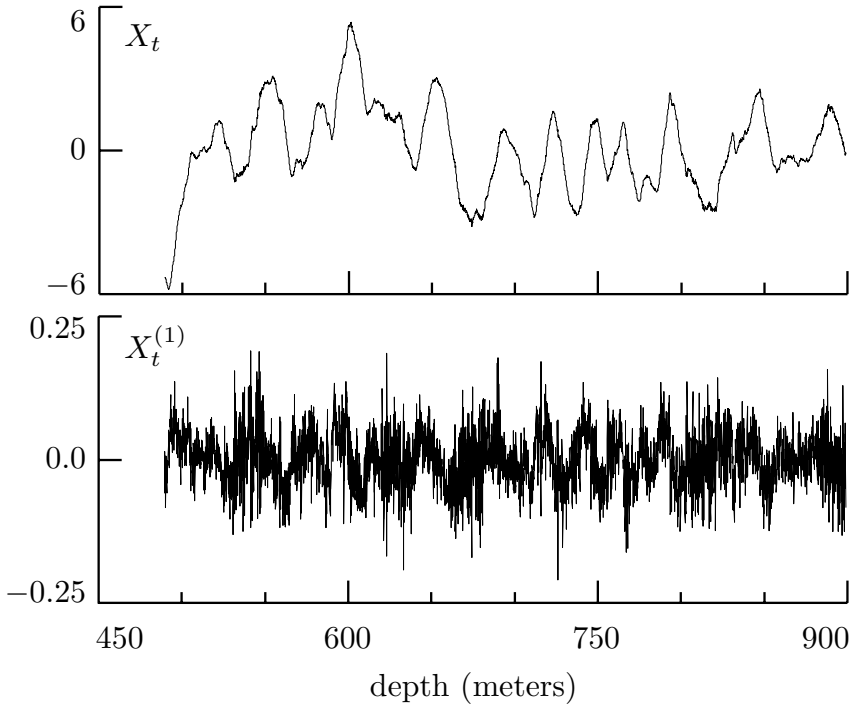

Figure 328. Selected portion $\{X_t\}$ of $N = 4096$ vertical shear measurements (top plot) and associated backward differences $\{X_t^{(1)}\}$ (bottom). The full series is plotted at the bottom of Figure 194, on which the subseries is delineated by two thin vertical lines.

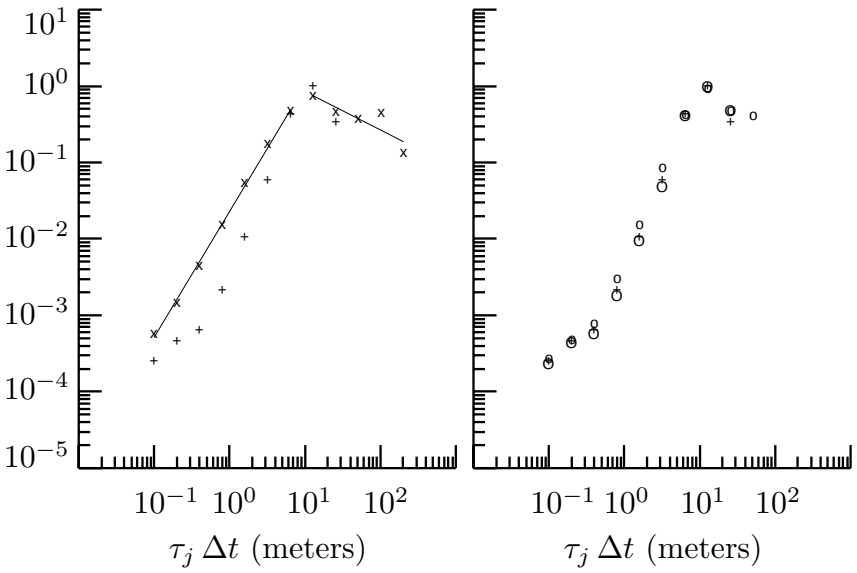

Figure 329. Wavelet variances estimated for vertical shear series using the unbiased MODWT estimator and the following wavelet filters: Haar (x's in left-hand plot, through which two regression lines have been fit), D(4) (small circles, right-hand plot), D(6) (+'s, both plots) and LA(8) (big circles, right-hand plot). The values for the various $\hat{\nu}_X^2(\tau_j)$ are listed on the Web site for this book – see page *xiv*.

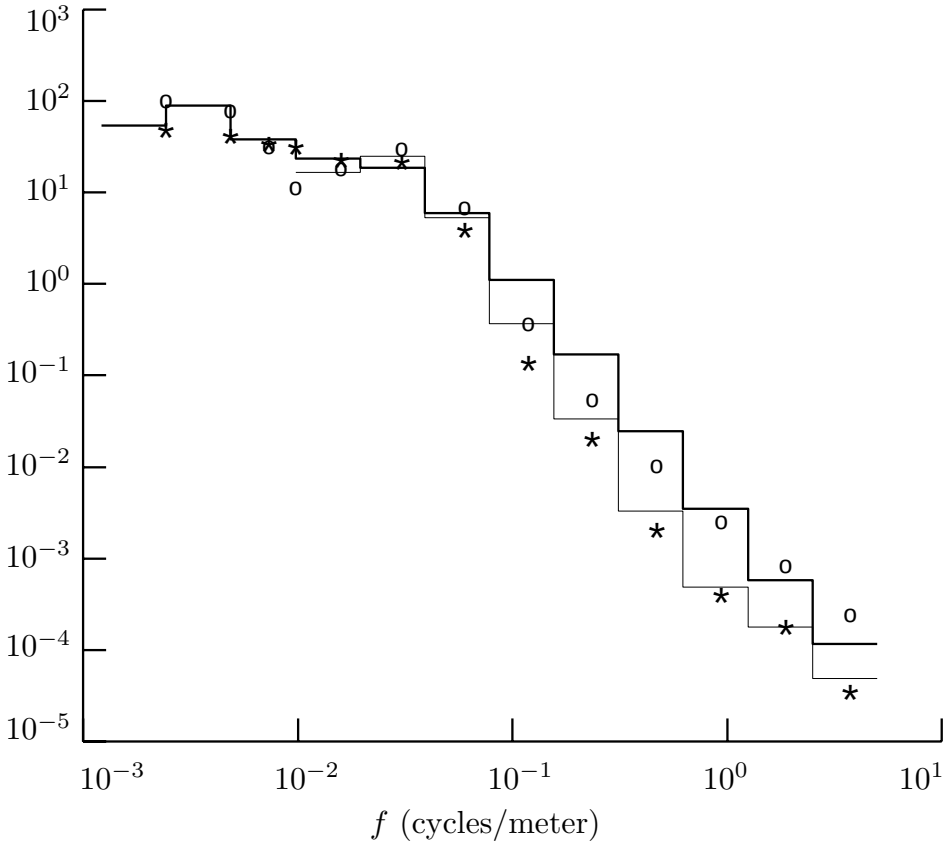

Figure 330. Comparison of 'octave band' SDF estimates for the vertical shear measurements based on the periodogram (o's), a multitaper SDF estimate formed using $K = 7$ sine tapers ($\star$'s) and Haar and D(6) wavelet variance estimates (thick and thin staircases, respectively). See text for details.

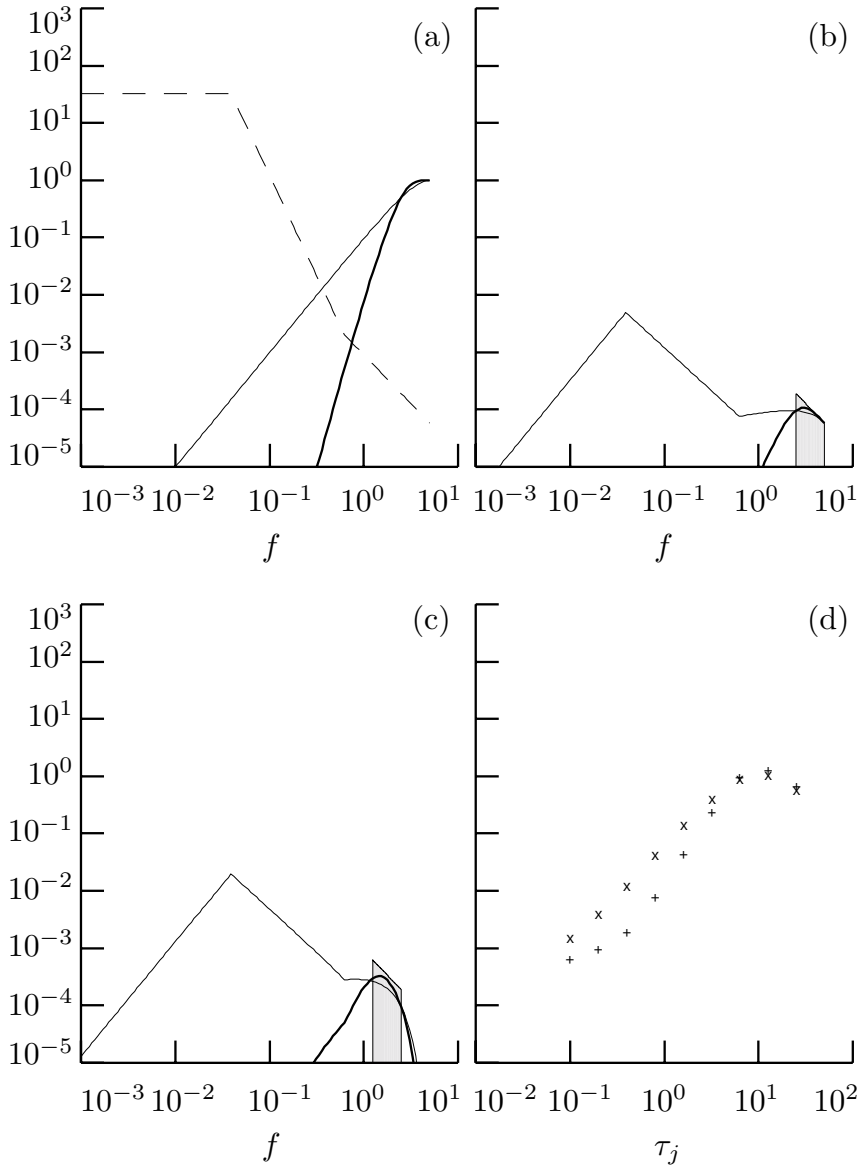

Figure 331. Leakage in Haar wavelet variance (see text for details).

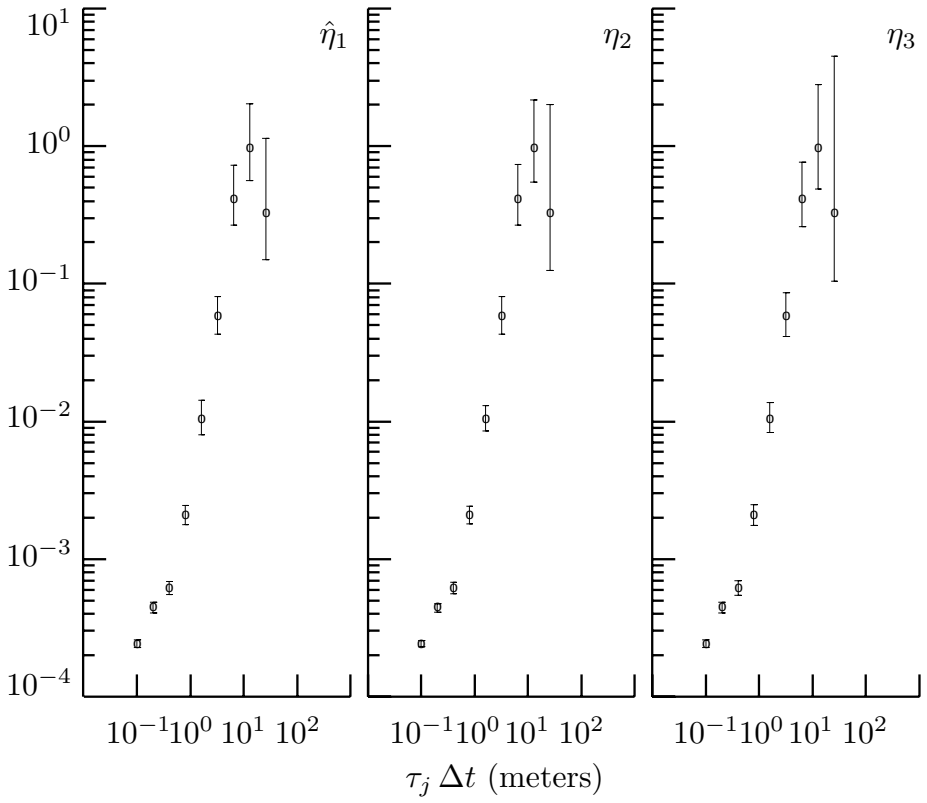

Figure 333. 95% confidence intervals for the D(6) wavelet variance for the vertical ocean shear series. The intervals are based upon the unbiased MODWT estimator (+'s in Figure 329 and o's above) and χ^2 approximations to its distribution with EDOFs determined by, from left to right, $\hat{\eta}_1$ of Equation (313d); η_2 of Equation (314b) using the nominal model for $S_X(\cdot)$ given by Equation (331); and η_3 of Equation (314c) (Table 333 lists the values for the EDOFs).

	j								
	1	2	3	4	5	6	7	8	9
$\hat{\eta}_1$	1890	1027	584	289	94	82	32	20	8
η_2	2850	1633	899	359	173	78	31	17	5
η_3	2046	1020	508	251	123	59	27	11	3
M_j	4091	4081	4061	4021	3941	3781	3461	2821	1541

Table 333. Equivalent degrees of freedom $\hat{\eta}_1$, η_2 and η_3 (rounded to the nearest integer) associated with the D(6) wavelet variance estimates $\hat{\nu}^2_X(\tau_j)$, $j = 1, \ldots, 9$, shown in Figure 333. The bottom row gives the number M_j of MODWT wavelet coefficients at each scale.

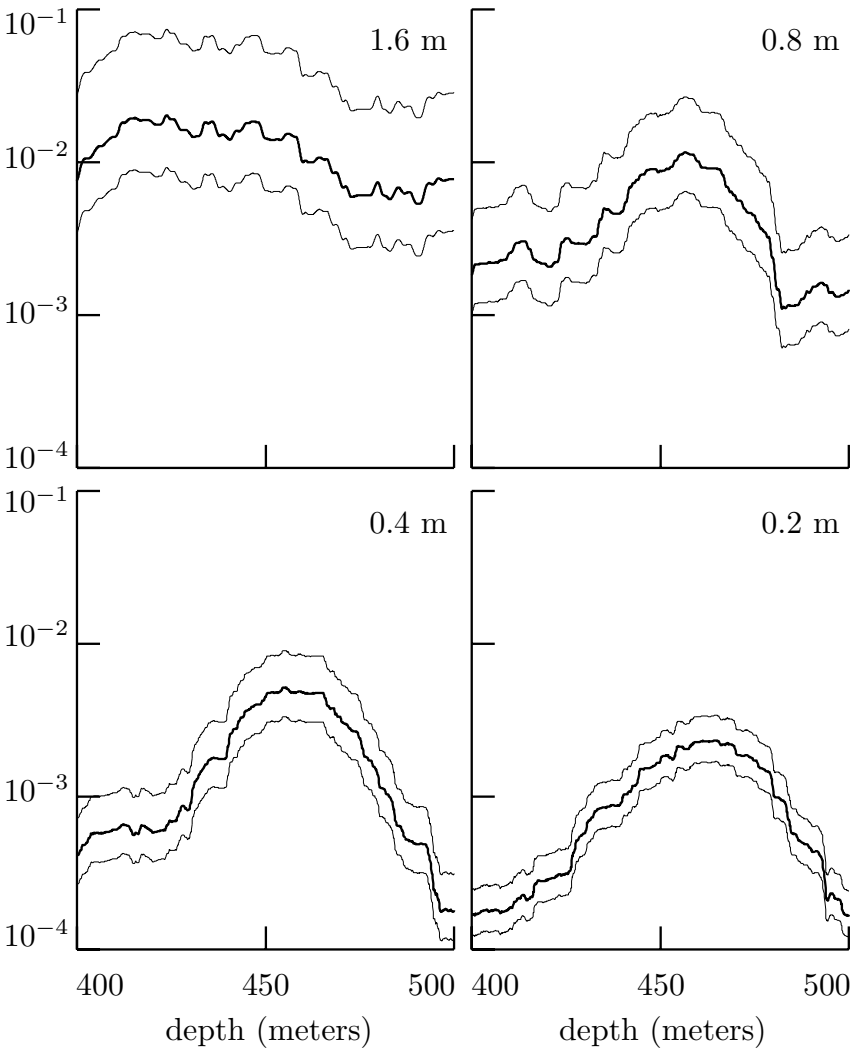

Figure 334. Estimated LA(8) wavelet variances (thick curves) for the shear data, computed using a running segment of 257 MODWT wavelet coefficients for depths surrounding 450 meters. As marked on the plots, the physical scales are 0.2, 0.4, 0.8 and 1.6 meters (i.e., $\tau_j \, \Delta t$, $j = 2, \ldots, 5$). The thin curves above and below the estimates are 95% confidence intervals as per Equation (313c) with $\eta = 257/2^j$ (this is in accordance with η_3 of Equation (314c)).